IEEE Access
Multidisciplinary | Rapid Review | Open Access Journal

Received May 14, 2019, accepted May 24, 2019, date of publication May 27, 2019, date of current version June 7, 2019.

Digital Object Identifier 10.1109/ACCESS.2019.2919493

The Impact of the Deformation Phenomenon on the Process of Lubricating and Improving the Efficiency Between the Slipper and Swashplate in Axial Piston Machines

GASTON HAIDAK, DONGYUN WANG, SHIJU E, AND FEIYUE LI
College of Engineering, Zhejiang Normal University, Jinhua 321004, China

Corresponding author: Dongyun Wang (zsdwdy@zjnu.edu.cn)

This work was supported in part by the National Natural Science Foundation under Grant 51205368, and in part by the Natural Science Foundation of Zhejiang Province under Grant LY17E050001.

ABSTRACT The process of lubricating a sliding interface between the Slipper and the swashplate in axial piston machines is a major solution for the improvement of its efficiency and performance. This lubrication process is largely influenced by the phenomenon of the thermoelastic and hydrodynamic deformation of the solid-liquid structure on this interface. This paper is mainly based on the study of the causes and processes of deformation, as well as the conditions of improvement of this deformation by the lubrication on the interface slipper/swashplate. For this, a mathematical model detailing the model deformation elastic and hydrodynamic on the slide interface Slipper/swashplate is made. The major parameters in the deformation such as the loads and the oil size are simulated. The energy equation is solved to understand the effect of the temperature on the oil behavior. The Reynold equation is solved to simulate the hydrodynamic pressure between the Slipper and the swashplate. A test rig is specially built to measure the torques and loads, the pressure, the oil height, and the temperature between the Slipper and the swashplate for different input conditions. The comparison between the simulation results and the experimental ones proves the coherence and the precision of the results of this research. Finally, some propositions to improve the performance of the axial piston machines for the lubrication mechanism on the Slipper/swashplate interface are given.

INDEX TERMS Axial piston machine, slipper-swashplate interface, efficiency improvement, lubrication mechanism, elasto-hydrodynamic deformation.

I. INTRODUCTION

The axial piston pump is currently an element whose demand is steadily growing on the market. Its popularity stems from its compactness, relative ease in controlling the effective fluid displacement per shaft revolution, and high pressure operation [1]. The interface between the Slipper and Swashplate is one of the most important interfaces in which a large part of the energy of the pump is lost. The performance loss mechanism on that surface is mainly caused by the thermo-elastic and hydrodynamic deformation of the Slipper/swashplate assembly. The thermo-elastic and hydrodynamic deformation of the Slipper is caused by several mechanisms occurring during the pump operation, in specific, from the Slipper and Swashplate dynamic motions to their deformations.

The Slipper performs several types of very complex movements on the Swashplate. Besides the macro motions governed by the pump kinematics, the Slipper also exhibits some micro motions such as a squeezing motion, tilting motion, and spinning motion, which are essential for the slipper operation [2]. Due to the multiple degrees of freedom on the macro and micro scales, the Slipper/swashplate interface is the most complicated lubricating interface in terms of dynamics [3]. Experimentally, Zhang *et al.* [2] investigated on the slipper spin and concluded that slipper spin occurs and its speed is approximately equal to shaft speed under test conditions. A tribo-dynamic model of the slipper bearing where the angular rate of the slipper spin was considered and the pressure

The associate editor coordinating the review of this manuscript and approving it for publication was Tao Wang.

governing equation has been proposed by Lin and Hu [4]; the effects of speed, pressure and oil viscosity on the oil film thickness of the slipper pair were investigated by means of this tribo-dynamic model. Iboshi and Yamaguchi [5] studied the Slipper bearing characteristics by deriving the Reynolds equation for the slipper bearing from the Navier-Stokes equation to evaluate the fluid film parameters of slipper, including tilting angle, maximum tilting angle azimuth and mean gap height. Chao *et al.* [6] derived the Reynolds equation for the slipper bearing in cylindrical coordinate systems using the differential analysis of fluid flow by evaluating the boundary condition of the Reynolds equation based on the slipper kinematics on the swashplate. They found that the Slipper does experience a translation in an elliptical manner rather than a plane rotation on the swashplate. Hooke and Kakoullis [7], Hooke and Li [8,] [10], Koç and Hooke [9] investigated the tilting behaviour and lubrication characteristics of the slipper bearing with different slipper running surface profiles theoretically and experimentally. They used the Reynolds equation to solve for the pressure distribution under the slipper land and thus the fluid force and moment acting on the slipper. According to their results, the fluid film thickness under the slipper land could be predicted with a reasonable accuracy through solving the force and moment equilibrium equations of the slipper. By analysing the solid body motion effect on the deformation on Slipper/swashplate interface, the Swashplate is not lifted out.

The behaviour of the swashplate, in addition to its inclination's angle, also influences the lubrication mechanism of the Slipper/Swashplate interface. The dynamic modelling of swashplate for conditions monitoring applications has been studied by Bedotti *et al.* [11]. Based on the equation of swashplate's motion, the pump regulators, the actuator torque, and the Karnopp friction model have been modelled. The torque characteristics for a swashplate-type seawater hydraulic axial piston motor has been investigated by Yang *et al.* [12] taking into account the dynamic pressure inside the piston chamber, the piston friction, and the pre-compressible angle. They found that an adequate pre-compression angle will not only ensure the isolation of piston chambers from any exchange ports, but also help diminish the pressure shock and the associate fluid noise.

The power loss on Slipper/swashplate interface is partially caused by fluid flow. The total power lost between Slipper and Swashplate is a summation of the power due to the force of the friction and that is due to the flow [13]. In order to improve the efficiency of piston pump, Gao et al. verified the accuracy of the hydraulic test rig using the deviation analysis method [14]. Rizzo *et al.* [15] applied a nanocoating (developed by ISTEC-C.N.R.) to the slippers of an axial piston pump to reduce the friction losses. This improved the pump overall efficiency map, which demonstrated that at low rotational speed, hydrodynamic lift causes power losses in terms of volumetric and mechanical efficiency due to the contrasting need to increase leakage to provide lubrication and to keep a minimum clearance in limit to limit the volumetric losses. Bergada *et al.* [16], Kumar *et al.*, Bergada and Watton [18] presented the expression for the leakage between the slipper and Swashplate, which took into account the slipper spin. The leakage expression was subsequently integrated into a differential equation to evaluate the instantaneous pressure in the displacement chamber. Grönberg [19] used a fluid structure interacting model called CASPAR to calculate a couple gap flow. He found that, the friction forces transmitted in the coupled gap flow module have a large impact on the power loss for low pump speeds with low pressure. However, the friction forces on the Swashplate/slipper interface increase the temperature of fluid by generating heat, and that heat generation causes a thermal deformation of the slipper and swashplate, which can also influence on the gap height between the slipper and the swashplate. Therefore, the thermal effect should be considered for the lubrication characteristics of slipper bearings [20]–[23]. The rising of temperature causes the decrease of fluid viscosity, which leads to the decrease of the fluid film thickness. And when the fluid film thickness is reduced between Slipper and swashplate, there is a greater chance that metal-metal contact occurs. Due to the tilting moment, the fluid film height distribution resulting from a rigid body separation of the slipper from the swashplate in the local slipper cylindrical coordinate system can be described using the height of the three control points at the outer diameter of the slipper [1], [13], [23], [24]. The deformation occurring on the Slipper/swashplate interface is due to the exchange and increase of heat between the solid-fluid structure and caused by the thermodynamic pressure under the Slipper. The fully coupled fluid-structure-thermal models established for slipper bearings to account for the thermal, elastic, and hydrodynamic effect [1], [25], [26] allowing the dependence of fluid pressure on structural deformation to be resolved as well as to update the temperature and viscosity of the fluid film. In order to make the research results more precise, several Slipper test rigs were built in various ways. The Slipper test rig has undergone a lot of modifications and can be classified into three categories [3], depending on the operations allocated as well as their operational approximation to that of the real pump. In order to improve the method of control of the hydraulic systems, Shen *et al.* [27] established an Integral Direct-drive Volume Control (IDDVC) electro-hydraulic servo system and found that compared to the conventional transfer model, the integrated model can precisely simulate the feature of dead-zone nonlinearity during positive and negative switchover motion; and Suzuki and Urata [28] developed a new design of pressure compensated flow control valve. Yu *et al.* [29] proposed VCR to denoise, fuse EWT components at different frequency bands, and enhance useful harmonic components in hydraulic pumps. At low rotational speed, hydrodynamic lift causes power losses in terms of volumetric and mechanical efficiency due to the contrasting need to increase leakage, to provide lubrication, and to keep a minimum clearance in order to limit the volumetric losses [25].

Relying on the large demand of axial piston machines for their multiple and various applications, it is understandable

that the lubrication solution of an important interface such as the Slipper/swashplate requires a more global and widespread study. The cause of hydrodynamic deformation of the Slipper and Swashplate are due to many factors such as the Slipper and Swashplate motion, the load on the Slipper, and the heat exchange between solids and liquids. In addition, the Swashplate moment and its dynamic angle regulation strongly effects the deformation and lubrication mechanism, and deserves greater research attention.

Therefore, the goal of the authors' research in this work is to discover the impact of the thermoelastic and hydrodynamic deformation and its lubrication mechanism on the slipper/swashplate interface. First of all, the mathematical model describing the kinematics and dynamics of the slipper and swashplate are studied, then the flow, pressure, and heat transfer equation on the slipper/swashplate interface are analysed. The second part presents the analytical and simulation models, where the numerical results are presented. The third part is the experimental part and the measurement of the data by a new test rig specially designed in the laboratory for measuring Fluid film thickness, temperature and, the axial forces under different applied loads. The fourth part presents a discussion and conclusion.

II. MATHEMATICAL MODEL

A. SLIPPER DYNAMIC MODEL/SLIPPER MOTION

1) SLIPPER MOTION

During the operation of the pump, due to swashplate inclination, shaft rotation, and piston forces, the slipper does not describe a circular motion on the swashplate. The spatial motion of the slipper is the combined movements of the rotation along with the cylinder and the reciprocating motion concerning the cylinder [2]. The mathematical equations of the Slipper motion under the Swashplate have been developed Yu *et al.* [30]. The instantaneous slipper velocity distribution in the slipper local cylindrical coordinate system can be defined for a given pump shaft speed, ω [1] can be rewritten as follows:

$$v_G = \begin{cases} v_{xG} = \omega \cdot \gamma_1 \cdot \cos(\gamma_1) \\ v_{yG} = \omega \cdot \gamma_2 \cdot \sin(\gamma_2) - (\omega.r.v_p) \end{cases} \quad \text{with} \quad (1)$$

$$\begin{cases} \gamma_1 = \sqrt{r^2 + r_G^2 - 2 \cdot r_G \cdot \cos(\pi - \theta)} \\ \gamma_2 = \dfrac{\pi}{2} - \cos^{-1}\left(\dfrac{\gamma_1^2 + r^2 - r_G^2}{2 \cdot \gamma_1 r}\right) \end{cases}$$

2) FLUID FILM THICKNESS

Following the action of the multiple forces exerted on the slipper, it is driven to perform many movements. Its slight rotation around the X-axis causes its inclination around the Y-axis, and vice versa. Following the pressure of the stocking, at any position given during the operation of the pump, the oil film between the slipper and the swash plate is wedge-shaped. The instantaneous lubricating oil film height h can be expressed as a function of three different points h_1, h_2, and h_3 on the outer edge with interval of 120° from each other [13];

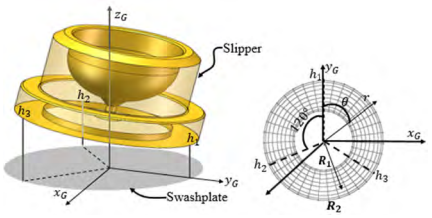

FIGURE 1. Wedge-shape of the oil film between the slipper and swashplate.

as shown in FIGURE 1. And the film thickness at an arbitrary point (r, θ) is calculated as follows:

$$h(r,\theta) = \frac{r \cdot cos\theta}{r_0 \cdot \sqrt{3}}(h_2 - h_3) + \frac{r \cdot sin\theta}{3 \cdot x_0}(2 \cdot h_1 - h_2 - h_3) + \frac{1}{3}(h_1 + h_2 + h_3) + \Delta l_{slp} - l_{swp} \quad (2)$$

where (r, θ) is the coordinate at the arbitrary point of the slipper in cylindrical coordinates, while r_0 is the reference radius. h_1, h_2 and h_3 are the height of the oil film in the three distributed points of the slipper, l_{slp} and l_{swp} are respectively the Slipper and Swashplate pressure/thermal deformation.

3) FORCES

The centrifugal force due to the shaft rotation is applied to the slipper/piston assembly [31]. The inclined external force pressing the bodies of the translational friction pair with a flat contact surface was analysed by Dobrov [32]. In TABLE 1, three references are defined: (XYZ), $(X_sY_sZ_s)$ and $(X_1Y_1Z_1)$ system are inertial systems. $(X_1Y_1Z_1)$ can be obtained by a rotation of (XYZ) system around the X-axis clockwise through an angle β. $(X_sY_sZ_s)$ defined in the center of gravity of the slipper, and the forces involved are illustrated. This set of forces, as presented below, rotate the assembly around the axis Z of the inertial reference (XYZ).

In FIGURE 2, F_{wKi} is the centrifugal force, F_{RKi} is the piston ball joint force, F_{DK} is the displacement chamber force, F_{TKi} is the force of the cylinder block, F_{aKi} is the inertia force, F_{TG} is the Slipper viscous friction force, (F_{SKyi}, F_{SKzi}) are the components of swashplate reaction force, and F_{RK} is

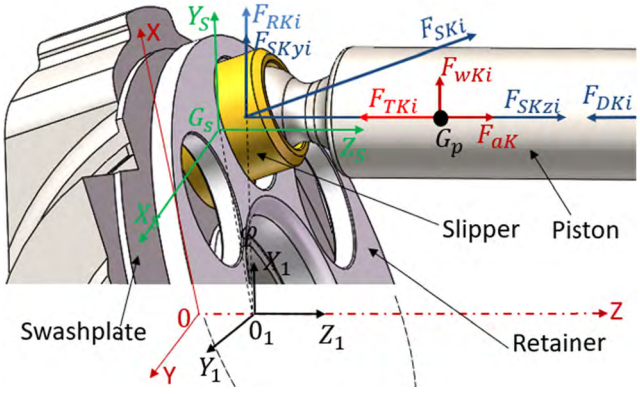

FIGURE 2. Free body diagram of slipper.

TABLE 1. The geometric characteristics and some operation conditions of the data used for the pump.

Parameters	Values	Parameters	Values
Radius cylinder block R_B [mm]	46	Diameter orifice slipper d_{DG} [mm]	2.5
Diameter bushing d_Z [mm]	24.125	Piston/Slipper mass assembly m_K [g]	48
diameter piston d_K [mm]	24	Length piston surface l_{KG} [mm]	37
length piston l_K [mm]	44	Mass of slipper m_G [g]	10
length bushing l_F [mm]	44	Shaft speed [rpm]	2500
Swash plate Angle β [deg]	16	Distance piston head-gap area l_G [mm]	7.6
Diameter orifice piston head d_{DK} [mm]	0.8	Length orifice slipper l_{DG} [mm]	3.48
Length orifice piston head l_{DK} [mm]	11.8	Inner diameter slipper d_{Gi} [mm]	15
Distance to the centre of mass of the piston/slipper assembly l_{SK}[mm]	31.9	Outer diameter slipper d_{Ga} [mm]	25

the resultant of piston/slipper assembly force. These forces have been mathematically modelled and expressed in detail by Haidak *et al.* [13], Wang *et al.* [33].

It is worth noting that the external forces exerted directly or indirectly on the Slipper have a considerable impact on the lubrication mechanism of the Slipper/swashplate interface in general and on the thermo-elastic deformation of Solids (Slipper and Swashplate) in particular. The slipper is loaded by primarily in the form of the resulting piston pressure force and secondary loads resulting from the contacts piston-cylinder board and spherical joint [25].

With regard to the behavior of the thickness of the fluid film at the bottom of the Slipper pocket, the influence of the load capacity exercising on the slipper must be taken into account. When the load on the slipper rises, the oil thickness decreases and the risk of having metal-to-metal contact is huge.

B. SWASHPLATE MOMENT

The swashplate moment is influenced by the fluid pressure coming from displacement chamber. The pressurized fluid in the displacement chamber exerts an axial fluid force on the piston/slipper assembly and generates a reaction force on the swashplate [34]. According to FIGURE 3, the force exerted

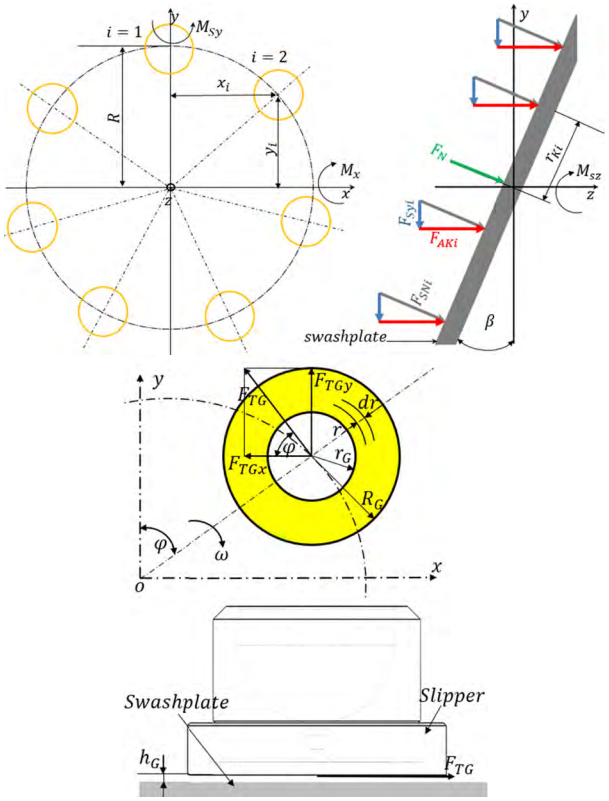

FIGURE 3. Forces and moments of the swashplate.

on the swashplate can be expressed as follows:

$$F_{AKi} = F_{DKi} + F_{aKi} + F_{TKi} \tag{3}$$

F_{DKi} is the pressure force depending on the instantaneous cylinder bloc pressure, and the components of the Swashplate's reaction force can therefore be subdivided according to axes and is expressed in Eq. (4).

$$F_{Sx} = 0; F_{Sy} = \sum_{i=1}^{Z} F_{Syi} = -tan\beta \cdot \sum_{i=1}^{z} F_{AKi}; \quad F_{Sy} = \sum_{i=1}^{Z} F_{AKi} \tag{4}$$

$$F_{TSi} = -F_{TGi} \quad F_{TSxi} = F_{vi}.cos\varphi i \tag{5}$$

F_N changes its origin during one shaft rotation. The friction force F_T exerted on the swashplate due to the slipper motion. The moments relating to the forces exerted on the swashplate are expressed as follows:

$$M_{Sx} = \sum_{i=1}^{n} R \cdot F_{AKi} \cdot cos\varphi_i \cdot \left(1 + tan^2\beta\right) = \frac{R}{cos^2\beta} \sum_{i=1}^{n} F_{AKi} \cdot cos\varphi_i \tag{6}$$

$$M_{Sy} = -R \cdot \sum_{i=1}^{n} F_{AKi} \cdot sin\varphi_i \tag{7}$$

$$M_{SZ} = \sum_{i=1}^{n} F_{Syi} \cdot x_{Si} + M_{TSi} = -R.\left(\sum_{i=1}^{n} F_{Tcj} + tan\beta \cdot \sum_{i=1}^{n} F_{AKi} \cdot sin\varphi_i\right) \tag{8}$$

Here, n represents the piston number. The swashplate moment in relation to X-axis is the sum of the moment of the

components of Swashplate forces in the directions of Y and Z (F_{TSi} and F_{Tzi}). Similarly, M_{Sz} is the moment due to Swashplate components in the directions of X and Z, given that the strength of the swashplate in the direction of the X is zero, its moment in the direction of Y is thus reduced to the moment derived from the component F_{Szi}. The components of the swashplate moment following the Z axe is normally the combination of the moment due to F_{Sxi}, F_{Syi} and the moment due to the friction force of Slipper F_{TG}; but it reduces to the two latest forces (F_{Syi} and F_{TG}) as F_{Sxi} is equal to zero in this case.

C. PRESSURE MODEL

1) FLUID FILM PRESSURE MODEL

The calculation of the pressure distribution between the Slipper and the Swashplate is one of the important works in predicting the lubrication of this interface. Thus, the fluid has an assumed Newtonian, viscous, incompressible, and laminar flow. For this, the equation of Reynold in cylindrical coordinates [26] can be discretised according to the shape of the base of the Slipper to calculate the pressure.

$$\frac{-1}{12r}\left(\frac{\partial}{\partial r}\left(\frac{r\cdot h^3}{\mu}\frac{\partial P}{\partial r}\right)+\frac{\partial}{\partial\theta}\left(\frac{h^3}{\mu r}\frac{\partial P}{\partial\theta}\right)\right)+\frac{1}{r}\frac{\partial}{\partial r}\left(\frac{r\cdot h\cdot v_{rt}}{2}\right)+\frac{1}{r}\frac{\partial}{\partial\theta}\left(\frac{h\cdot v_{\theta t}}{2}\right)-v_{rt}\frac{\partial h_t}{\partial r}-\frac{v_{\theta t}}{r}\frac{\partial h_\theta}{\partial\theta}+\frac{\partial h_t}{\partial\theta}-\frac{\partial h_\theta}{\partial t}=0 \tag{9}$$

μ is the oil viscosity, h is the fluid film thickness, and P is the fluid pressure; Eq. (9) can be solved numerically using the Finite Volume Discretization method as it can be seen in FIGURE 4. Due to the fact that the finite volume mesh is structured, the cell centroids are located such that the connection between each neighbour is exactly orthogonal to the shared cell face, so the face pressure differentials of Eq. (9) can easily be represented discretely as in Eq. (10).

$$\frac{\partial P_e}{r\partial\theta}=\frac{P_E-P_P}{r\Delta\theta},\quad \frac{\partial P_w}{r\partial\theta}=\frac{P_P-P_W}{r\Delta\theta},\quad \frac{\partial P_n}{\partial r}=\frac{P_E-P_P}{\Delta r},\quad \frac{\partial P_s}{\partial r}=\frac{P_P-P_S}{\Delta r} \tag{10}$$

2) DISPLACEMENT CHAMBER MODEL

The pressure in the displacement chamber acts directly on the forces of the piston as illustrated in the FIGURE 5. So, the instantaneous pressure, P_{DC} can therefore be modelled using a separate lumped parameter approach and is fully determined before the calculation of this model, and considered as a transient boundary condition. This

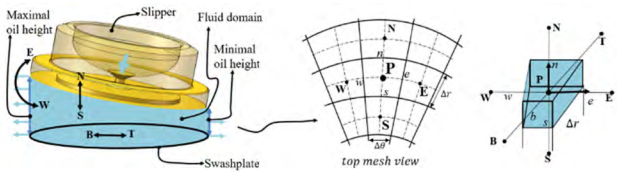

FIGURE 4. Slipper/swashplate fluid film Finite volume discretization scheme.

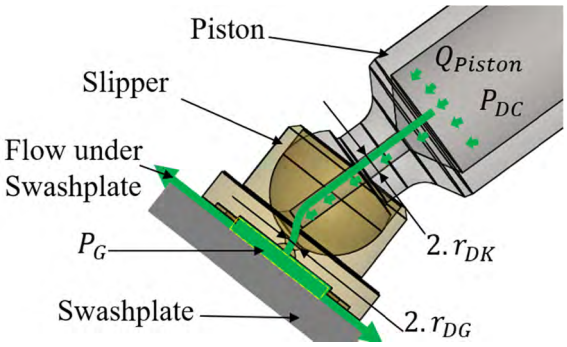

FIGURE 5. Sketch of slipper pocket pressure control volume.

pressure is governed by the following pressure build-up equation [16], [34].

$$\frac{dP_d}{dt}=\frac{K}{V}\left(Q_r-Q_{SS}-Q_{PB}-Q_{BV}-\frac{dV}{dt}\right) \tag{11}$$

In Eq. (11), K stands for the bulk modulus of the fluid, V is the volume of the displacement chamber, and Q_r represents both the flow inlet and outlet of the displacement chamber during respectively motoring mode and pumping mode. As the displacement chamber transitions from discharge to suction pressure, the hydrostatic pressure boundary, and resulting deformation changes by significant magnitudes. To correctly account for the contribution of transient deformation change to Reynolds squeeze pressure, a backwards difference method is used [26].

$$\frac{\partial l_{slp}}{dt}=\frac{l_t^{slp}-\delta_{t-\Delta t}^{slp}}{\Delta t};\quad \frac{\partial l_{slp}}{dt}=\frac{l_t^{swp}-l_{t-\Delta t}^{swp}}{\Delta t} \tag{12}$$

δ_{slp} and δ_{swp} are respectively the slipper and Swashplate pressure/thermal deformation. Given that the deformation referenced here is due to pressure, Eq. (12) can be modified such that the Slipper deformation becomes a direct function of pressure, and it shows that stationary deformation can fluctuate and contribute to the compression effects if the deformation of the cyclic plateau does not move with the slippers, due to transient variations in the total amplitude of the oil pressure acting the Swashplate.

3) THE SLIPPER POCKET PRESSURE MODEL

The pressure of the fluid at the bottom of the Slipper is a pressure due to fluid flow. It is the flow coming from the displacement chamber noted Q_{piston} which can be calculated using the orifice equation. The flow by the lubrication gap Q_{SG} can be calculated by integrating the velocity of the fluid around the circumference of the Slipper [26].

$$P_G=P_{G,t-1}+\Delta t\cdot\frac{K}{V_{pocket}}\left(Q_{piston}-Q_{SG}-\frac{dV_{pocket}}{dt}\right) \tag{13}$$

Eq. (13) is identified as the pressure distribution under slipper, where K is bulk modulus and V_{pocket} is oil pocket volume as it is illustrated in FIGURE 5.

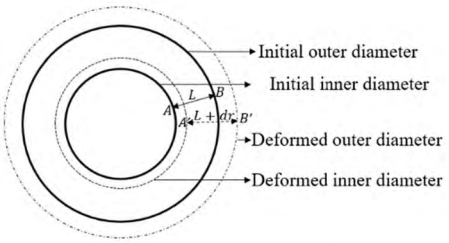

FIGURE 6. Illustration of 2D elastic slipper deformation.

D. THE FLOW ANALYSIS

The fluid flow analysis in the axial piston pump focuses on three different areas, such as the flow in the displacement chamber, the flow below the Slipper pocket, and the flow between the Slipper and the swashplate. The leakage formula on the Slipper/swashplate interface developed in the generic form by Bergada *et al.* [16], Kumar *et al.* [17] can then be used and integrated according to the value of k_1 in Eq. (14).

$$Q_{slipper-swashplate} = \int_0^{2\pi} \frac{k_1}{12\mu} d\theta_s \tag{14}$$

E. THERMOELASTIC AND HYDRODYNAMIC DEFORMATION

1) SOLID BODY DEFORMATION

The slipper deformation in this case is due to the oil film pressure distribution along the radius direction. To solve this issue, the generic pressure distribution of a slipper with any total lands number developed by Bergada *et al.* on reference [35] can be rewritten as:

$$P = P_{inlet} - \frac{\Delta P}{\sum_{i=1}^{i=n} \frac{1}{h_1^3} ln\left(\frac{r_{i+1}}{r_i}\right)} \left[\frac{1}{h_i^3} \cdot ln\left(\frac{r}{r_i}\right)\right] \tag{15}$$

'n' represents the number of lands, ΔP is the difference between the outlet and inlet pressure, r_i is the ith land radius, r is the arbitrary radius point, and h_i is the fluid film thickness between the slipper and swashplate at the ith point.

The points A and B represent the small infinitesimal element of the slipper. They were initially separated by a distance L and $(L + dr)$ after a deformation. Thus, the local elastic deformation equation [23] can be modified and rewritten for slipper with multi-lands as:

$$\delta_e(r_i) = \frac{\left(1 - \vartheta_e^2\right)}{\pi.E} \frac{1}{L} \left[P_{inlet} - \frac{\Delta P}{\sum_{i=1}^{i=n} \frac{1}{h_1^3} ln\left(\frac{r_{i+1}}{r_i}\right)} \left[\frac{1}{h_1^3} \cdot ln\left(\frac{r_A}{r_i}\right)\right]\right] \tag{16}$$

Eq. (16) represents the elastic deformation equation at point A. To find the deformation equation at point B, the distance L should be expressed as follows:

$$L = \begin{cases} \sqrt{r_j^2 + r_i^2 - 2 \cdot r_j \cdot r_i cos\theta_k} & r_j > r_i \\ \sqrt{r_j^2 + r_i^2 + 2 \cdot r_j \cdot r_i cos\theta_k} & r_j < r_i \end{cases} \tag{17}$$

θ_k represents the circular angle at the point A. By substituting Eq. (17) in Eq. (16), the elastic deformation equation at the point B can be found as follows:

$$\delta_e(r_i) = \frac{\left(1 - \vartheta_e^2\right)}{\pi.E} \sum_{j=1}^{m+1} \times \sum_{k=1}^{n} \frac{P_{inlet} - \frac{\Delta P}{\sum_{i=1}^{i=n} \frac{1}{h_1^3} ln\left(\frac{r_{i+1}}{r_i}\right)} \left[\frac{1}{h_1^3} \cdot ln\left(\frac{r_A}{r_i}\right)\right]}{\sqrt{r_j^2 + r_i^2 \pm 2 \cdot r_j \cdot r_i \cdot cos\theta_k}} \tag{18}$$

δ_e is a local vertical deformation of point P and ϑ_e the Poisson's ratio, E is the Young's modulus, r_A is a slipper radius at point A, and L is the initial distance between A and B.

The elastic deformation of the solid bodies (Slipper and Swashplate) show that deformation is linear and substantially influences the lubrication mechanism of the Slipper/swashplate interface. This elastic deformation can be calculated by solving the elasticity equation. The elasticity equation with appropriate boundary conditions is an applicable model of solid deformation [26].

$$\nabla.\sigma(x, y, z) = 0 \tag{19}$$

$$G(u, \overline{u}) = -\int_V \overline{u}(\nabla \cdot (\sigma)b)dV \tag{20}$$

$$G(u, \overline{u}) = \int_V \overline{\varepsilon}^T D\varepsilon dV - \int_A \overline{u}^T t dA - \int_V \overline{u}^T b dV = 0 \tag{21}$$

$$u \cong a^T h, \quad \overline{u} \cong a^T h \tag{22}$$

σ is a stress, 'h' are basis functions, and 'a' is the weight; the finite element method with solid four-nodded tetrahedral elements. The method of residuals is used to solve Eq. (24) by introducing into the weak form in Eq. (25). Then, the Galerkin method of weighted residual in Eq. (25) can be used to reduce the infinite dimension formulation of Eq. (26)

2) PRESSURE DEFORMATION EQUATION

The contact between the Slipper and the swashplate is not in dry contact a result of the existence of the oil film expressed above in Eq. (1). The elastic deformation mentioned here is the elastic linear deformation. This deformation is assumed to be in the linear elastic regime. Although deformation can change rapidly in response to varying pressure loads, the scale of variation is significantly less than the speed of sound in elastic solids and thus no steady terms are neglected for the solid body analysis [26].

When the fluid film thickness deviation becomes less than the critical film thickness, the solid body pressure is created and the viscous body friction between solid-liquid acts simultaneously. This influences the lubrication mechanism of the Slipper/swashplate interface.

3) THE HEAT TRANSFER MODEL AND SOLID'S ELASTIC DEFORMATION

Viscous friction within the lubricant causes localized heating, and due to high thermal conductivity, boundary surface

temperatures have a strong impact on the fluid temperature. The temperature of the fluid plays an important role in the lubrication of the Slipper/Swashplate interface and it is calculated using energy equation defined in Eq. (27).

$$\nabla \cdot (\rho, c_P, v, T) = \nabla \cdot (\lambda \nabla T) + \left[\left(\frac{\partial v_r}{\partial z} \right)^2 + \left(\frac{\partial v_\theta}{\partial z} \right)^2 + \frac{4}{3} \left(\frac{v_r}{r} \right)^2 + \left(\frac{v_\theta}{r} \right)^2 \right] \quad (23)$$

The viscosity of the fluid depends on the temperature of the fluid as it can be seen in Eq. (34), where T_f is the film temperature. When the temperature rises, the viscosity decreases; simultaneously the flow increases. This is a huge loss of energy. Eq. (28) gives the link between the dynamic viscosity of oil and the temperature, where a and b are constants.

$$\mu = a \cdot e^{-b.T_f} \quad (24)$$

The boundary conditions for the solution of the energy equation according to the height of the fluid between the Slipper and the Swashplate are described as follows:

Radially, the temperature of the fluid is elevated to the area or the thickness between the Slipper and the Swashplate is minimal, and smaller in the area or the thickness between the Slipper and the Swashplate is maximal (Figure 4). Following the Z-axis, the fluid temperature is equal to that of the swashplate when z = 0 and equal to that of the Slipper pad for z according to function f defined in FIGURE 7.

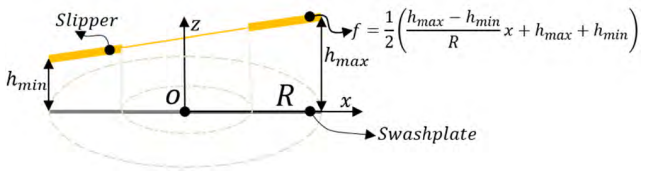

FIGURE 7. Temperature boundary condition.

The determination of the solid bodies' temperature fields is based on a finite volume discretization. The diffusive-convective form of the energy equation in solid body can be expressed in differential form and its governing equation for conductivity heat transfer is as follows:

$$\nabla \cdot (q) = 0 \text{ with } q = -\lambda \nabla \mathrm{T} \quad (25)$$

Here, λ is the thermal conductivity of the solid material. Similarly, to the elasticity one described in part II.E. 1) from Eq. (23) to Eq. (25), the global form can be converted into a weak variational formulation. The Galerkin method of weighted residuals will then be used in conjunction with a finite element approximation to solve the scalar temperature field [19]. The weak form of the conductivity heat transfer equation can be written as follows:

$$G(T, \vec{T}) = \int_\Omega T(\lambda \nabla \mathrm{T}) d\Omega = 0 \quad (26)$$

Ω represents the domain. The boundary of the definite solution domain is separated into two different parts, S_1 and S_2. S_1 is the temperature boundary condition. S_2 are the other boundary conditions including heat flux, heat convection, and heat ratio.

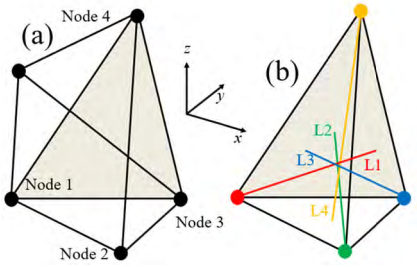

FIGURE 8. Unstructured mesh configuration for four nodded tetrahedron element (a) and tetrahedron natural coordinates (b).

Here, the solid is discretized into many individual finite element method and Eq. (29) can be applied to each element volume individually. In FIGURE 13, it can be seen how the Slipper domain has been discretized into the sum of many individual tetrahedral shaped volumes; and each element volume is illustrated by the four-node linear tetrahedron shaped volume presented in FIGURE 8. Four natural coordinates (L_1, L_2, L_3, L_4) are defined for the tetrahedron with the coordinates values respectively (1,0,0,0), (0,1,0,0), (0,0,1,0) and (0,0,0,1). It is important to emphasis that the tetrahedron are not necessarily coplanar. For the thermal conductivity analysis, the temperature is assumed to be a weighted linear combination of the four nodal temperature; so that the temperature of a point with natural coordinates (L_1, L_2, L_3, L_4) is interpolated as in Eq. (31.a), and the temperature field within the tetrahedron is expressed on Eq. (31.b).

$$T_P = [L_1, L_2, L_3, L_4] \cdot \begin{Bmatrix} L_1 \\ L_2 \\ L_3 \\ L_4 \end{Bmatrix} (a)$$

$$T(x, y, z) = [N_1, N_2, N_3, N_4] \cdot \begin{Bmatrix} T_1 \\ T_2 \\ T_3 \\ T_4 \end{Bmatrix} (b) \quad (27)$$

Eq. (27) (a) and (b) represent respectively the temperature of a point with natural coordinates and the temperature field within the tetrahedron. Thus, the boundary condition usable for temperature analysis is that of mixed convection; For which the magnitude of heat flux is directly proportional to the difference between the temperature of Slipper and the temperature of swashplate surface. This difference is proportional to the heat transfer convective coefficient.

III. ANALYTICAL AND SIMULATION PARTS

A. PARAMETERS AND INPUT CONDITIONS

For the simulation entirety made in this work, the geometrical characteristics and certain operating conditions of the data used for the pump as well as the characteristics of the fluid

TABLE 2. Characteristics of the fluid.

Parameters	Values
Kinematic viscosity P coefficient P_c1[-]	1.5e-13
Kinematic viscosity weighting factor w [-]	0.9000
Kinematic viscosity T coefficient T_c1[-]	9.6310
Kinematic viscosity P coefficient P_c2 [-]	2.1025
Kinematic viscosity T coefficient T_c2 [-]	3.7873
Dynamic oil viscosity [Pa.s]	0.073
Density oil at reference point [kg/m^3]	1048
Volumetric thermal expansion coefficient [1/K]	05.76e-4
Thermal conductivity of oil [W/m.K]	0.037
Heat capacity of the oil [J/kg.K]	2000

and the material properties of slipper and Swashplate are described in the following tables:

The oil used for the simulation is a natural viscous oil whose characteristics are given in Table 2; and T defines the temperature.

B. COMPUTATIONAL TECHNICS

In order to properly analyse the lubrication mechanism of the Slipper/swashplate interface in the axial piston pump, the preceded mathematical formulations are used for the simulation, and the procedure diagram is presented in FIGURE 9. In the first part, the values of h_1, h_2, and h_3 are arbitrarily attributed to the beginning of simulation to obtain preliminary

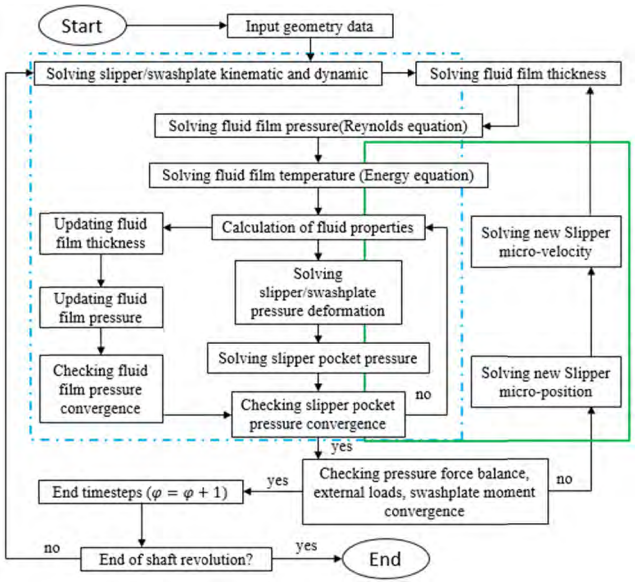

FIGURE 9. Flow chart of the complete proposed numerical simulation model.

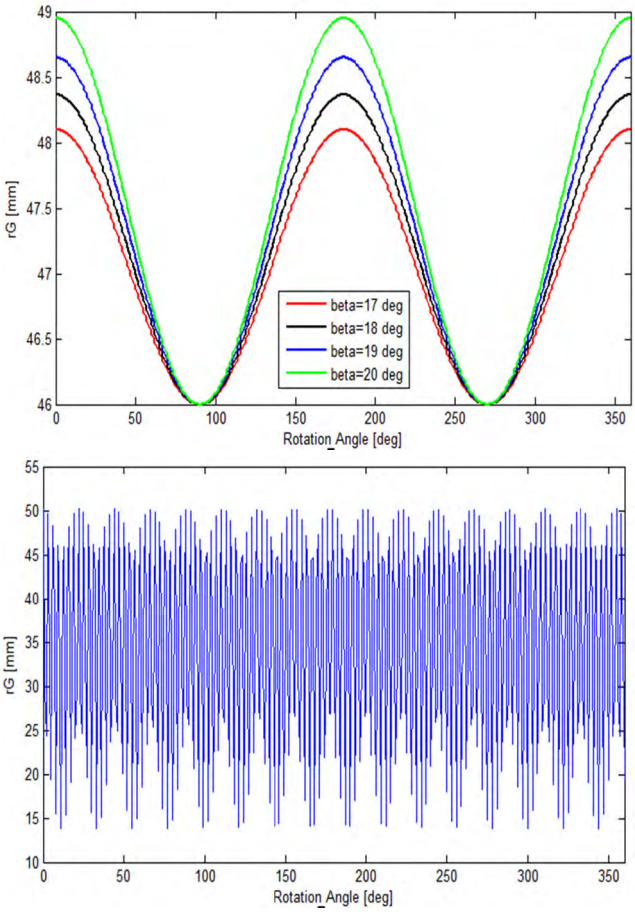

FIGURE 10. The instantaneous radius of the slipper centre from the swashplate centre.

distribution of the fluid. Nevertheless, the dependence of the fluid pressure on the structural deformation is resolved, as is the updating of the temperature and viscosity of the fluid film. For the following, Newton's iterative method can be used to find a Slipper micro velocity which brings the fluid pressure under the slipper into balance with the external loads in the second calculation loop by regenerating and improving the accuracy of the results.

IV. RESULTS

A. SLIPPER MOTION EFFECT

The speed of the Slipper is unstable at the very beginning of the operation of the pump, and begins to stabilize over time. The evolution of the speed of the Slipper in function of the angle of rotation of the shaft. The instantaneous radius of the slipper centre from the swashplate centre denoted r_G as a function of shaft angle is simulated and given in FIGURE 10. r_G is simulated as a function of the shaft rotation angle for four different values of the Swashplate angle beta; the effect of the Swashplate angle on the Slipper instability can be seen on the left part of FIGURE 10. The right hand of FIGURE 10 represents r_G for beta equal to 20 degree, including its micro-motion.

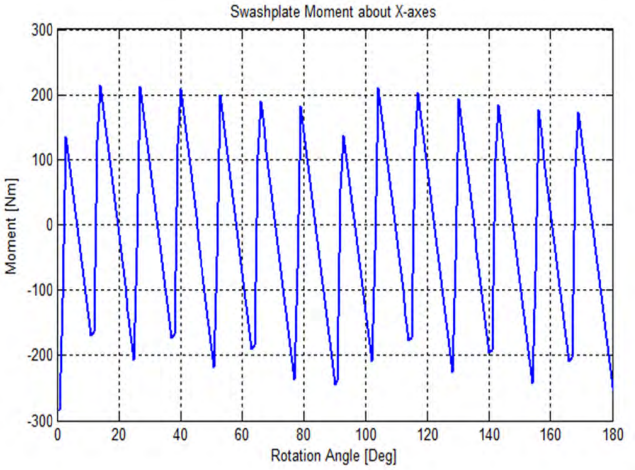

FIGURE 11. Swashplate moment in X-axis.

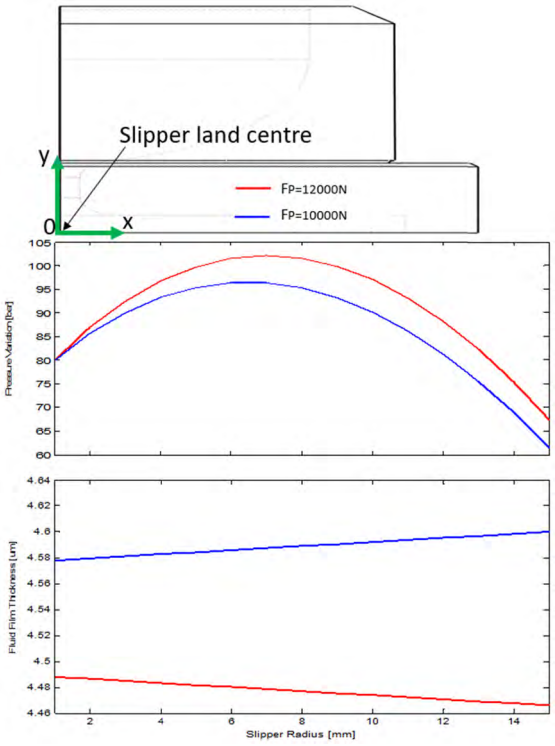

FIGURE 12. Slipper pocket pression and fluid film variation.

B. THE EFFECT OF SWASHPLATE MOMENT

In the case of pumps with a variable displacement Swashplate, the moment relative to the X-axis is not only coming from the structure, but also from the its control system due to the angle regulator which is pushing periodically the swashplate under the barrel plates. The swashplate is loaded by multiple pistons in the high and lower pressure zone

The load applied on the Slipper/Swashplate interface greatly influences the lubrication phenomenon. For a very high load, the pressure is high and the thickness of one between the Slipper and the swashplate is minimal.

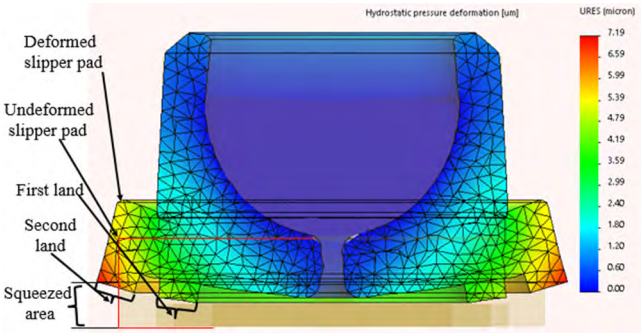

FIGURE 13. Hydrostatic pressure deformation of two lands slipper.

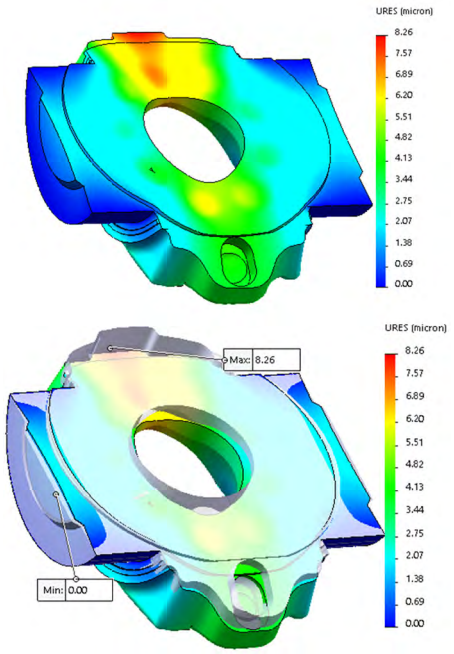

FIGURE 14. Single swashplate pressure deformation/superposed to the non deformaed.

FIGURE 12 illustrates the variation of the pressure film and oil height between the pocket of the Slipper and the swashplate for two different loads.

C. THE EFFECT OF HYDROSTATIC PRESSURE ON THE SOLID BODY DEFORMATION

Since the Slipper is an external pressurized bearing, the hydrostatic pressure field alone will cause a significant deformation of the surface and the hydrostatic deformation would affect not only the hydrodynamic pressure due to the movement of the Slippery, but it will affect the hydrostatic pressure field itself [26]. The Guyuan reduction method which is applicable for linear elastic and static models neglecting inertial forces has been proposed by Hashemi *et al.* [25]. However, the effect of the inertial force in the lubrication mechanism of the Slipper/Swashplate interface is very important, which can be computed before the computational process.

TABLE 3. The material proprieties of slipper and swashplate.

Proprieties	*Slipper*	*Swashplate*
Material	Copper alloys	Cast steel
Mass density [kg/m^3]	8500	7300
Thermal conductivity [W/m.K]	110	38
Specific heat [J/kg.K]	390	440
Poisson's ratio [N/A]	0.33	0.26
Sher modulus [N/ m^2]	3.7e+10	7.8e+10
Elasticity modulus [N/ m^2]	1e+11	1.9e+11
Yield strength [N/ m^2]	2.396e+8	2.412e+8

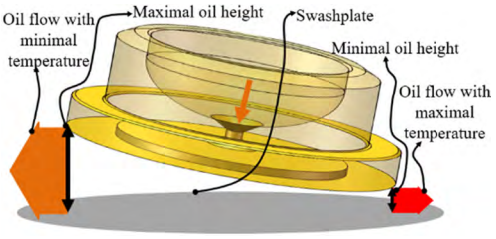

FIGURE 15. Slipper position for the calculation of oil temperature.

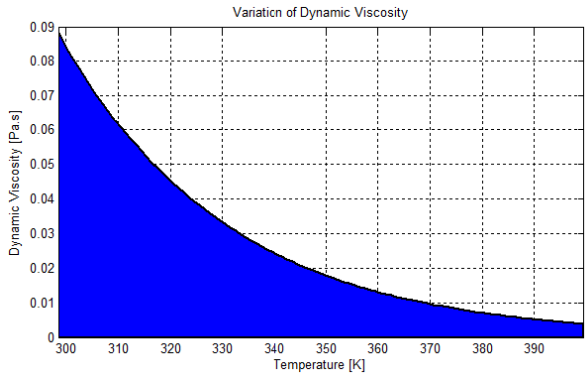

FIGURE 16. Dynamic viscosity of oil.

TABLE 4. The types of sensors used for the experimental part.

Type of sensor	Description
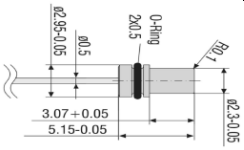	**DISPLACEMENT SENSOR** Temperature stability: ≤0.025%FSO/°C Connection: integrated coaxial cable 0.25m (ø 0.5mm) with solder connection board Pressure resistance (static): front 2000bar / rear side splash water Maximum operating temperature: 150°C Housing material: ceramic
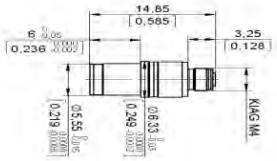	**PRESSURE SENSOR** Pressure range up to 250 bar (3 626 psi) • Membrane optimized for thermal transients and small sensor size • Extremely wide operating temperature range
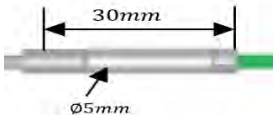	**TEMPERATURE SENSOR** Extension cable: -PE sheath: 2.5 mm - 85°C -PTFE sheath: 2.5 mm -200°C

The hydrodynamic, inertial, and swashplate reaction forces can be calculated by the formulas developed by Haidak *et al.* [13] in order to be applied in the simulation process and boundary conditions. The swashplate reaction and hydrodynamic forces applied respectively on the slipper lands and the Slipper pocket.

The particular case here is the Slipper has two lands. The mesh used is the tetrahedral one; each tetrahedral element has four non-coplanar nodes with a specified connectivity. To perform the analysis, a pressure of 315 bar is applied under the pocket of the Slipper, and the hydrostatic pressure deviation can be observed in FIGURE 13. The outer part of the surface of the second land of the Slipper is the part undergoing more compression. This is explained by the last two terms of Eq. (9). These terms represent the normal velocity of the slipper and swashplate surfaces, and it is due to the squeeze action (bearing surfaces move perpendicular to each other).

The swashplate uses for the simulation is that a variable angle. The characteristics material used are defined on Table 3. During the operation of the pump, many of the forces are applied to the swashplate which is taking support on the bearings. In addition to its inclination and to the control mechanism of its angle, its deformation is less accentuated on the supported areas (plain bearing size). Following the pressure exerted by the loads of all the pistons on it by the slipper, the swashplate undergoes a non-uniform deformation which can be interpolated and calculated. In addition to pressure deformation, that due to temperature followed by the local deformation must also be taken into account. To achieve this analysis, the constraints are applied on the two plains bearing. The temperature distribution in the lubricating film can be solved by the convective-diffusive scalar transport equation defined by Eq. (27).

The area of high elastic deformation varies in function of the inclination of the swashplate and the quantity of

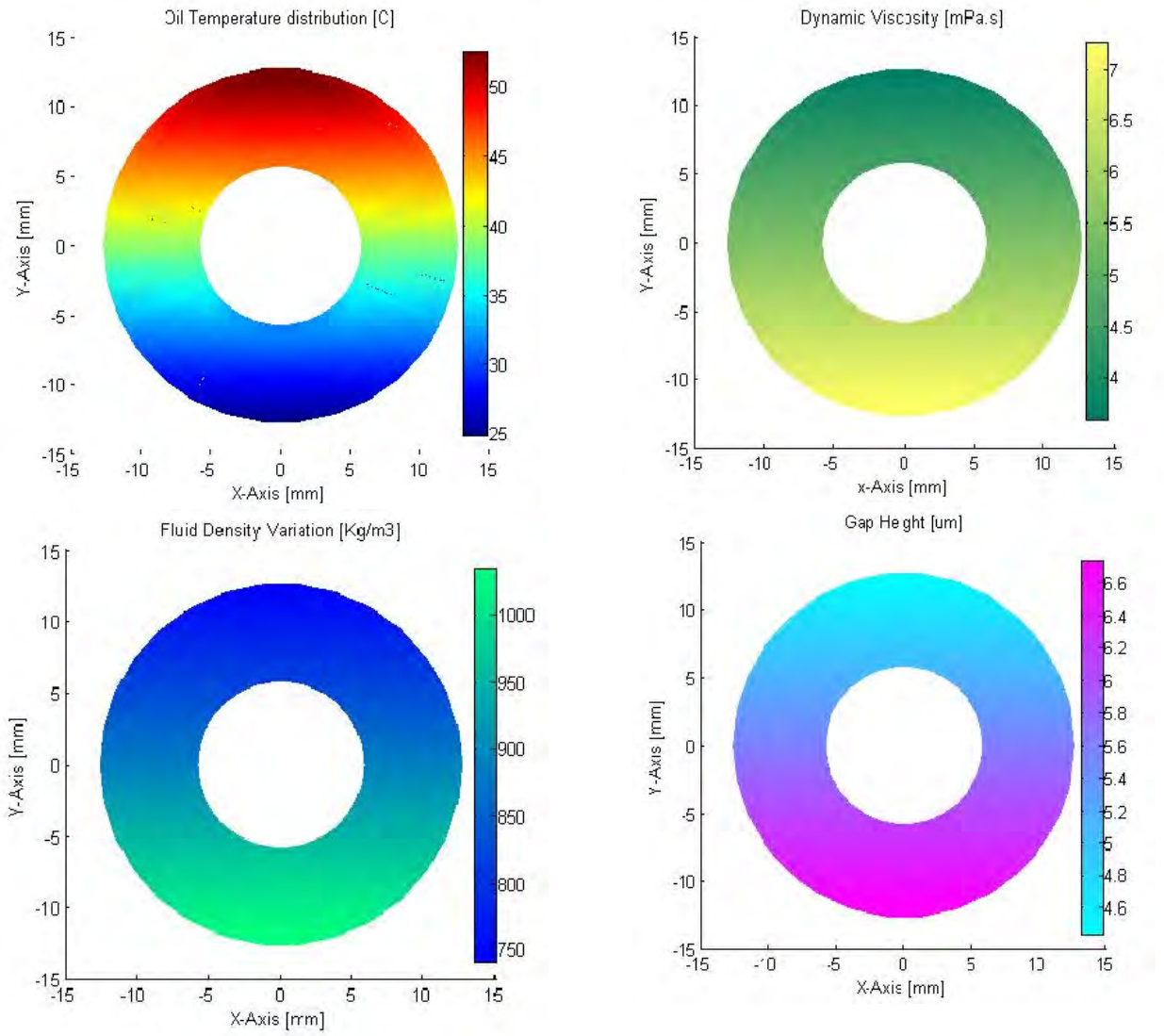

FIGURE 17. Distribution of temperature, density, dynamic viscosity and gap height of oil under slipper.

load (pressure force) applied, and also by what the lubricant domain itself is moving.

D. THE EFFECT OF HEAT EXCHANGE ON FLUID

The effect of heat transfer between solid-liquid on the Slipper/Swashplate interface is one of the most complex and delicate phenomena in the lubrication mechanism of the Slipper/Swashplate interface. The viscous friction forces, in addition to the loads applied on the Slipper, creates an increase in the temperature between solid-liquid. As the Slipper motion on the swashplate is dynamic, and taking into account the deformation caused by thermal expansion and hydrostatic pressure loads, the oil film thickness between the Slipper and Swashplate is not uniform at under the Slipper land. When the oil temperature is lowered, the increase in temperature becomes more pronounced [36]. The oil thickness between the Slipper land's size subjected to the greatest load and the swashplate is minimal (see illustration in FIGURE 15). Thus, the fluid temperature increases when the oil thickness between the two solids (Slipper and swashplate) decreases.

The fluid viscosity is a vital property of the fluid; it is directly linked to the temperature. When the fluid temperature increases, the viscosity decreases. And when the viscosity decreasing, the leakages between the Slipper and the Swashplate increases and the oil thickness decreases. This phenomenon is delicate because it can lead to metal-metal contact and in addition, when the oil thickness is very small, the thermo-elastic deformation becomes larger. The variation of the viscosity of the fluid in function of the temperature present in FIGURE 16 is calculated using the formula of the equation described in part II-E.1), and the ambient dynamic viscosity oil is as given in Table 2 (0.073 Pa.s). As well as viscosity, the density of the fluid depends largely on the temperature and they all have high influence on the load carrying capacity of the Slipper pad.

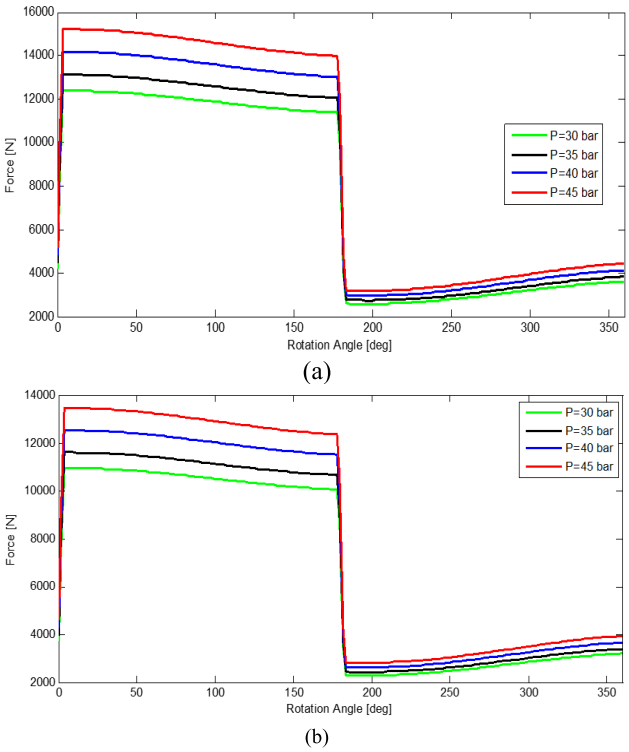

FIGURE 18. Slipper pad primary loads variation. (a) Primary load for n = 1000 RPM. (b) Primary load for n = 2000 RPM.

Considering the inclination angle of the slipper is very small, the pressure and temperature will be higher near the inner edge of the sealing earth with a large deformation of the thickness of the oil film. This can cause the oil thickness of the interior edge of the slipper's ground to be convex. But for some important values of the slipper tilting angle, these behaviours of the film of oil on the edges are not the same.

The fluid used for the simulation is that of which the characteristics are described in Table 2. For the heat distribution in the fluid, the heat diffusion equation described in Eq. (30) is solved. For this simulation part, the Slipper with a land is considered. The temperature distribution, the viscosity, the density, and the thickness of oil between the slipper and the swashplate are illustrated in FIGURE 17.

E. LOADS AND HYDRODYNAMIC PRESSURE EFFECTS

The thermoelastic deformation of the components (Slipper and Swashplate) is mainly due to the operation with their poorly lubricated interface, and this causes a huge loss of energy. The range of values in which the fluid film thickness must belong for optimal lubrication has been previously studied by Haidak *et al.* [13]. There is a minimal critical value below which the risk of having metal-metal contact is wide [25]. Increasing the speed of shaft rotation can play a big role in adjusting the oil thickness variation.

All the forces applied to the Slipper pad are represented in the form of a load which has a significant effect in the deformation phenomenon on the Slipper/swashplate interface. To fully understand how the slipper pad is loaded,

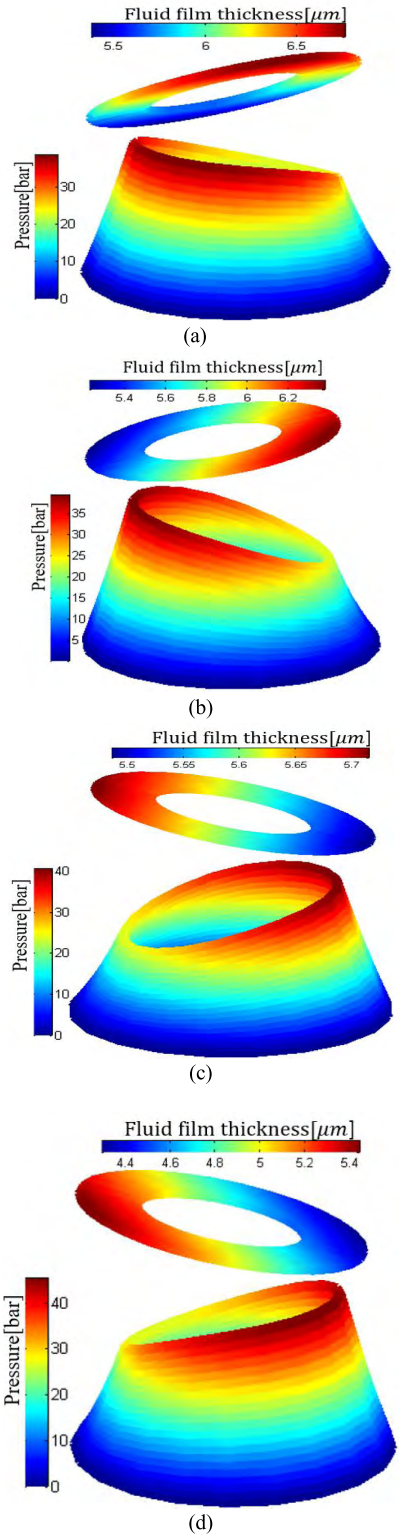

FIGURE 19. Slipper/swashplate interface simulated unwrapped dynamic pressure and fluid film thickness field over one shaft revolution, for four different values of pocket pressure and with n = 1000 RPM. (a) Supplied pressure value 30bar. (b) Supplied pressure value 35bar. (c) Supplied pressure value 40bar. (d) Supplied pressure value 45bar.

the mathematical equations of the primary loads in the form of the resulting piston pressure developed in reference [25] are used to calculate the slipper pad load for four different

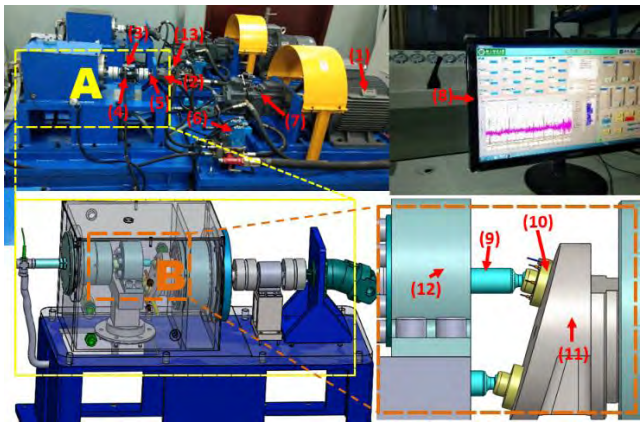

FIGURE 20. The 3D and real slipper test bench set-up in its environment.

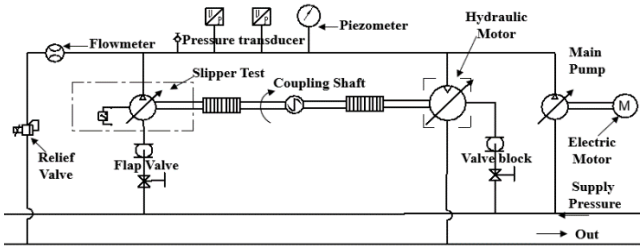

FIGURE 21. Steady state testing circuit.

values of the supplied load and two (1000 RPM, 2000 RPM) shaft rotation speeds as presented in FIGURE 18 FIGURE 18.

The effects of loads on the lubrication mechanism is well observable on the hydrodynamic pressure simulated in FIGURE 19. Due to the hydrodynamic motion of Slipper, the hydrodynamic pressure deformation influencing the distribution of the oil thickness on the Slipper/swashplate interface can then be observed. The region with a high-pressure value contains the smallest value in the oil height.

The hydrodynamic and squeeze motion of Slipper is characterised by the pressure distribution form. The fluid film thickness field is not a strict wedge-shaped plane.

V. EXPERIMENT MEASUREMENT

To verify the accuracy of our simulation results, the rig test was designed, allowing us to measure the temperature and the oil size between the Slipper and the swashplate. The pressure of the Slipper pocket and the torque moments are also measured in the operation conditions. FIGURE 21shows the SteadyState testing circuit of the test rig.

In FIGURE 20, (A) is the Slipper test rig, (B) is the Main part of the Slipper test rig, (1) Electric motor, (2) hydraulic motor, (3) hydraulic hose, (4) Torque sensor, (5) shaft (6) Electromagnetic relief valve, (7) main pump, (8) computer and requisition data, (9) Piston, (10) Slipper, (11) Swashplate, (12) Cylinder block, (13) Compensated flow control valve.

In this test rig, the rotor is the swashplate, it rotates with the shaft, and the cylinder block is the stator. The main pump provides pressure oil for the test pump and motor. The motor drives the swashplate shaft through the coupling and torque

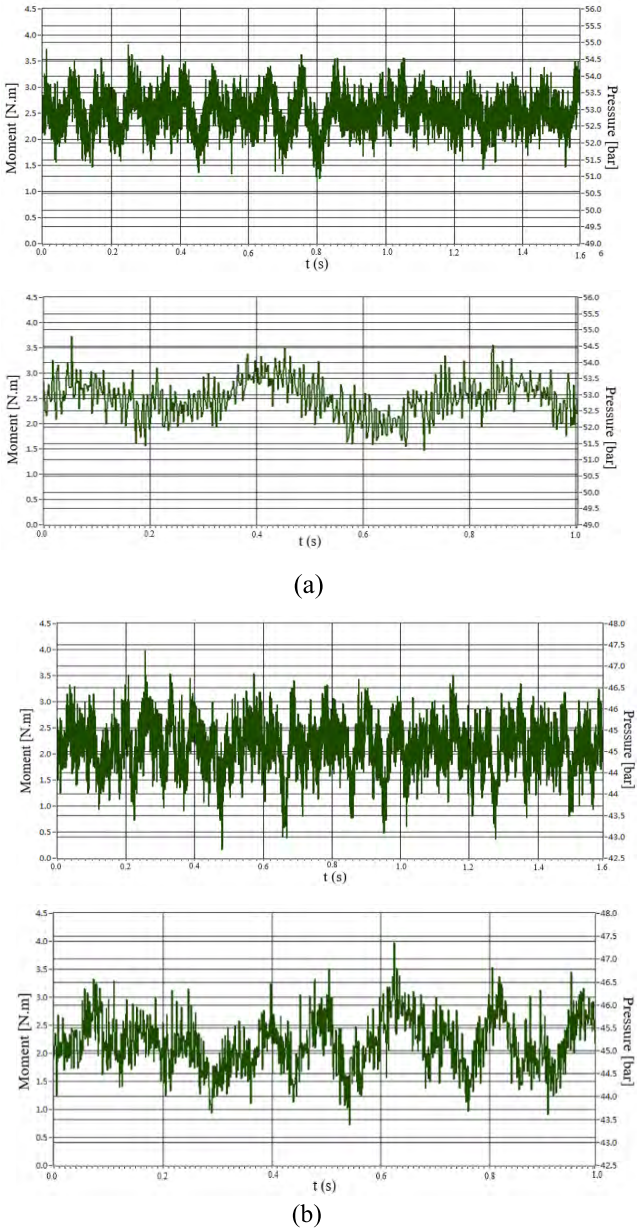

FIGURE 22. Experimental results of pressure between slipper and swashplate under running condition, versus time (s). (a) Supply load is 50 bar. (b) Supply load is 40 bar.

meter to realize reciprocating movement of the Slipper/piston asembly. The torque meter collects the torsional moment during the movement of the motor. The electromagnetic relief valve helps to change the supply pressure, and the pressure oil for the piston chamber by the oil pipeline.

The whole slipper piston assembly used here for the experimentation is specifically designed based on the quantity and qualities of the sensors to be inserted. A total of six sensors are inserted into the Slipper pad and a pressure sensor inserted into the Slipper pocket. Among these six sensors inserted in the Slipper pad, three are the displacement sensors that are placed on the same circular line and separated by 120 degrees from each other. These sensors are used to capture

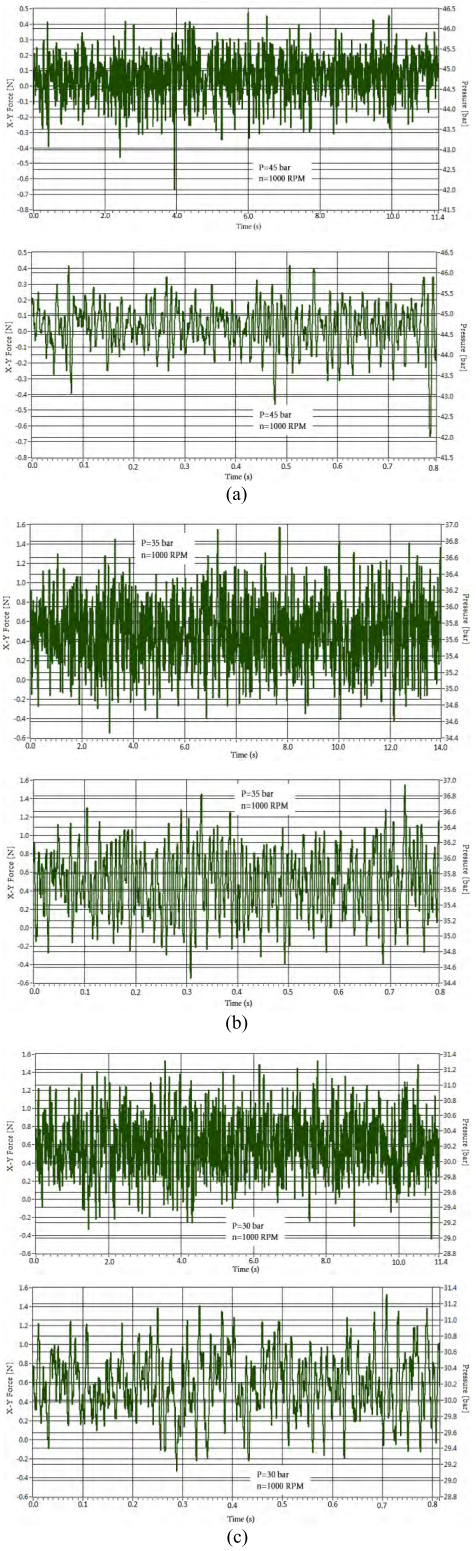

FIGURE 23. The output pressure and force at n = 1000 rpm. (a) Supplied pressure P = 40 bar. (b) Supplied pressure P = 35 bar. (c) Supplied pressure P = 30 bar.

the oil height between the Slipper and the Swashplate. The other three sensors are the temperature sensors which are places similarly to those of the displacement. These last three are places to capture the fluid temperature data between the

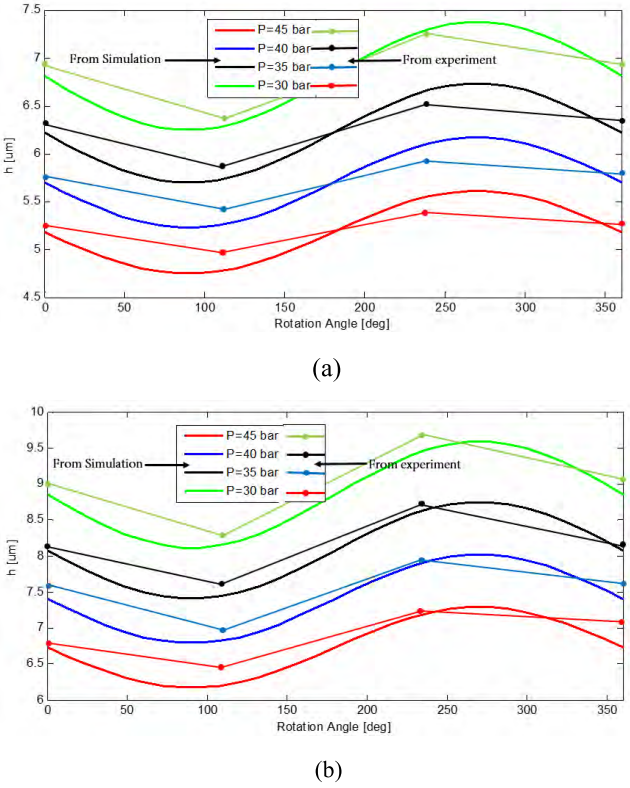

FIGURE 24. Fluid film thickness for one rotation shaft. (a) For a speed of speed of 1000 RPM. (b) For a speed of 1500 RPM.

Slipper and the swashplate. A pressure sensor is placed under the Slipper pocket to retrieve the data on the fluid pressure in the Slipper pocket. The same test is repeated several times, while exchanging the speed of rotation of the shaft and the supplied pressure in order to determine the effect of loads on the temperature and height of oil.

For different applied load and rotation speed of the shaft, the pressure and the shaft torque are visualized in FIGURE 22. FIGURE 23 presents the variation of the pressure and the axial force for different values of rotation's speed, and load. The figures from FIGURE 22(a) to FIGURE 23(c) each shows the distribution for a large time and for a short time.

FIGURE 24 demonstrates the circumferential distribution of the estimated fluid film thickness between slipper and swashplate. For the experimental conditions, the height values are taken for five different values of the supply pressure. As a first step, the shaft rotation is fixed at 1000 RPM (FIGURE 24(a)), and also for the same values of the supply pressure with a shaft rotation speed of 1500 RPM (FIGURE 24 (b)). The oil temperature in the cylinder is 30°, and the viscosity of the fluid is 0.0735 *Pa.s*.

To get the experimental data of the temperature, the rig test set is initialised and the measurements are made for four different values of loads (45, 40, 30 and 25 bar). For each load-applied value, four different values of the shaft rotation speed (600, 1000, 1500, and 2000 RPM) are changed. The taking of the temperature data is carried out by the

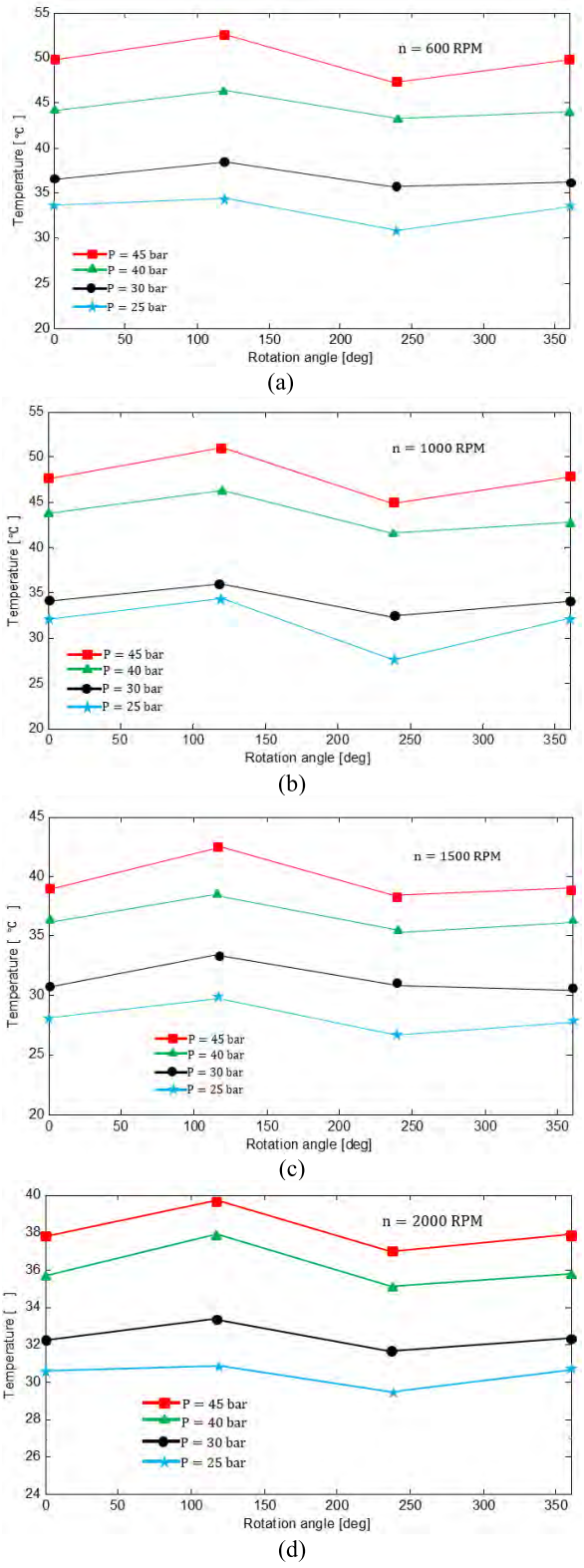

FIGURE 25. The measured fluid temperature between Slipper/swashplate. (a) For n = 600RPM. (b) For n = 1000RPM. (c) For n = 1500 RPM. (d) For n = 2000 RPM.

three different sensors for each value of the shaft rotation speed. Thus, for each applied load, four data Sockets are performed corresponding to the four different rotation speeds. The temperature shape of the curves based on the data collected on the computer from the three different sensors is given in FIGURE 25 for the different shaft rotational speeds.

VI. DISCUSSION

The instantaneous radius of slipper Centre from the shaft centre vary unstably between 46 and 50 mm; this proves the non-circularity movement of the Slipper on the swashplate, which is one of the sources of possible contact or deformation on the Slipper/swashplate interface

Experimentally, the results of measurement show more clearly the effect of the load and the temperature on the lubrication mechanism. The difference in pressure for the two different loads (50 and 40 bar) is approximately 14.5 and 15 bar, respectively. For the four different values (30, 35, 40, and 45 bar) of the supplied pressure, the pressure distribution is approximately (37, 38, 48, 42, and 48 bar) respectively; these values justify the results obtained in the simulation part. For each these supplied pressures, the value of h is given. The respective values of h for these supplied pressures in order are respectively (6.6, 6.2, 5.8, and 5.4 μm). These results mean that for a large value of load, h is small. The same values of supplied pressure used for simulations in part IV. IV-E are also used for experimental measurement, and the results are given on FIGURE 23. In the same way, the values of the fluid temperature are measured and FIGURE 24 clearly demonstrates the load effect and the speed of the shaft rotation on the temperature evolution.

The value of the temperature is high when the load value is large. The temperature is slightly higher than the first half-turn (between 0 and 180 degrees) the shaft rotation angle, while the value of h is at the minimal. This directly translates the impact of the pressure (load) on the oil thickness between the Slipper and the Swashplate.

VII. CONCLUSION

In this paper, a thermoelastic and hydrodynamic deformation model mainly based on the load's effects for the Slipper/swashplate interface of Axial piston machines has been presented. This model considers several physical parameters involved in the deformation mechanism influencing the Slipper/swashplate interface fluid film performance in terms of fluid-structure and thermal interactions. The mechanical parts' elastic deformation problems are solved. The parameters involved in the process and the mechanism of the thermoelastic and hydrodynamic deformation on the Slipper/swashplate interface are mathematically and analytically studied. More attention is paid on the influence of load on the behaviour of the fluid structure. The Slipper and Swashplate motion, the fluid film thickness fields, the pressure distribution fields, and the temperature fields are solved. The elastic deformation due to the effect of the hydrostatic pressure of slipper and Swashplate are simulated. The influence of Slipper load on the oil film thickness is analysed for several shaft rotation speeds, and the hydrostatic pressure deformation of the slipper and Swashplate are made. This experimental

study has been conducted to measure and compare the torque and the Slipper load carrying capacity under different shaft rotation speeds, the axial forces, the fluid film thickness, and the oil temperature between the Slipper and the Swashplate under different supplied loads. The results obtained in the simulation part are well verified by the experimental results. From all the results ensuing from this research, the following conclusions and suggestions can be drawn:

(1) The preliminary origin of the deformation phenomenon on the Slipper/swashplate interface is the nature of the movements of the solid (Slipper/swashplate) components, due to the fact that the instantaneous radius of slipper Centre from the shaft centre vary unstably (between 45-50mm).

(2) The load set exerted on the Slipper by reducing the oil height to cause a large deformation can be adjusted by increasing the speed of rotation of the shaft. The elevation of the fluid temperature on the Slipper/swashplate interface is due to the heat exchange between the solid bodies and the fluid by the friction forces.

(3) The dynamic viscosity, density, and fluid size are the parameters determined by the lubricant that decrease with the increase of the temperature on the Slipper/swashplate interface. When the temperature rises by 40K, the dynamic viscosity of the oil decreases of 0.061$Pa.s$.

(4) The insertion of a good retained from the Slipper is solution. The Swashplate's angle regulator largely influences the Swashplate's elastic deformation. The result of elastic deformation on the diametrically opposed areas of the angle regulator is higher (from 5-8μm).

REFERENCES

[1] A. T. Schenk, "Predicting lubrication performance between the slipper and swashplate in axial piston hydraulic machines," Ph.D. dissertation, Dept. Agricult. Biol. Eng., ProQuest, Purdue Univ., Ann Arbor, MI, USA, Jan. 2014, pp. 1–179.

[2] J. Zhang, Q. Chao, Q. Wang, B. Xu, Y. Chen, and Y. Li, "Experimental investigations of the slipper spin in an axial piston pump," *Measurement*, vol. 102, pp. 112–120, May 2017.

[3] Q. Chao, J. Zhang, B. Xu, Q. Wang, and H. Huang, "Test rigs and experimental studies of the slipper bearing in axial piston pumps: A review," *Measurement*, vol. 132, pp. 135–149, Jan. 2019.

[4] S. Lin and J. Hu, "Tribo-dynamic model of slipper bearings," *Appl. Math. Model.*, vol. 39, no. 2, pp. 548–558, Jan. 2015.

[5] N. Iboshi and A. Yamaguchi, "Characteristics of a slipper bearing for swash plate type axial piston pumps and motors: 4th Report, effects of surface roughness," *Bull. Jpn. Soc. Mech. Eng.*, vol. 29, no. 254, pp. 2539–2546, 1986.

[6] Q. Chao, J. Zhang, B. Xu, and Q. Wang, "Discussion on the reynolds equation for the slipper bearing modeling in axial piston pumps," *Tribology Int.*, vol. 118, pp. 140–147, Feb. 2018.

[7] C. J. Hooke and Y. P. Kakoullis, "The effects of non-flatness on the performance of slippers in axial piston pumps," *Proc. Inst. Mech. Eng., C, J. Mech. Eng. Sci.*, vol. 197, no. 4, pp. 239–247, Oct. 1983.

[8] C. Hooke and K.-Y. Li, "The lubrication of slippers in axial piston pumps and motors–the effect of tilting couples," *Proc. Inst. Mech. Eng., C, J. Mech. Eng. Sci.*, vol. 203, no. 5, pp. 343–350, Sep. 1989.

[9] E. Koç and C. J. Hooke, "Considerations in the design of partially hydrostatic slipper bearings," *Tribology Int.*, vol. 30, no. 11, pp. 815–823, Nov. 1997.

[10] C. Hooke and K.-Y. Li, "The lubrication of overclamped slippers in axial piston pumps—Centrally loaded behaviour," *Proc. Inst. Mech. Eng., C, J. Mech. Eng. Sci.*, vol. 202, no. 4, pp. 287–293, Jul. 1988.

[11] A. Bedotti, M. Pastori, F. Scolari, and P. Casoli, "Dynamic modelling of the swash plate of a hydraulic axial piston pump for condition monitoring applications," *Energy Procedia*, vol. 148, pp. 266–273, Aug. 2018.

[12] L. Yang, S. Nie, S. Yin, J. Zhao, and F. Yin, "Numerical and experimental investigation on torque characteristics of seawater hydraulic axial piston motor for underwater tool system," *Ocean Eng.*, vol. 104, pp. 168–184, Aug. 2015.

[13] G. Haidak, D. Wang, E. Shiju, and J. Liu, "Study of the influence of slipper parameters on the power efficiency of axial piston pumps," *Adv. Mech. Eng.*, vol. 10, no. 9, Sep. 2018, Art. no. 168781401880146.

[14] M. Gao, H. Huang, X. Li, and Z. Liu, "A novel method to quickly acquire the energy efficiency for piston pumps," *J. Dyn. Syst., Meas., Control*, vol. 138, no. 10, Jun. 2016, Art. no. 101004.

[15] G. Rizzo, G. P. Massarotti, A. Bonanno, R. Paoluzzi, M. Raimondo, M. Blosi, F. Veronesi, A. Caldarelli, and G. Guarini, "Axial piston pumps slippers with nanocoated surfaces to reduce friction," *Int. J. Fluid Power*, vol. 16, no. 1, pp. 1–10, Feb. 2015.

[16] J. M. Bergada, S. Kumar, D. L. Davies, and J. Watton, "A complete analysis of axial piston pump leakage and output flow ripples," *Appl. Math. Model.*, vol. 36, no. 4, pp. 1731–1751, Apr. 2012.

[17] S. Kumar, J. M. Bergada, and J. Watton, "Axial piston pump grooved slipper analysis by CFD simulation of three-dimensional NVS equation in cylindrical coordinates," *Comput. Fluids*, vol. 38, no. 3, pp. 648–663, Mar. 2009.

[18] J. Bergada and J. Watton, "Force and flow through hydrostatic slippers with grooves," in *Proc. 8th Int. Symp. Fluid Control, Meas. Vis.*, 2005, pp. 1–8.

[19] D. Grönberg, "Prediction of case temperature of axial piston pumps," Dept. Appl. Mech. Division Fluid Dyn., Chalmers Univ. Technol., Gothenburg, Sweden, Tech. Rep., p. 72.

[20] K. Tang, S. Wilson, S. Y. Yeung, S. Katzer, and S. Tisherman, "119: Managing albumin use in the intensive care unit using a collaborative approach," *Crit. Care Med.*, vol. 44, no. 12, p. 107, Dec. 2016.

[21] H.-S. Tang, Y.-B. Yin, Y. Zhang, and J. Li, "Parametric analysis of thermal effect on hydrostatic slipper bearing capacity of axial piston pump," *J. Cent. South Univ.*, vol. 23, no. 2, pp. 333–343, Feb. 2016.

[22] Y. D. Tang, H. J. Shen, X. F. Zhang, G. F. B. Yun, Z. Y. Peng, and X. Y. Liu, "Effect of annealing on the characteristics of Ti/Al ohmic contacts to p-Type 4H-SiC," *Mater. Sci. Forum*, vol. 897, pp. 395–398, May 2017. Accessed: Dec. 17, 2018. [Online]. Available: https://www.scientific.net/MSF.897.395

[23] H. Tang, Y. Ren, and J. Xiang, "A novel model for predicting thermoelastohydrodynamic lubrication characteristics of slipper pair in axial piston pump," *Int. J. Mech. Sci.*, vols. 124–125, pp. 109–121, May 2017.

[24] C. Shi, S. Wang, X. Wang, and Y. Zhang, "Variable load failure mechanism for high-speed load sensing electro-hydrostatic actuator pump of aircraft," *Chin. J. Aeronaut.*, vol. 31, no. 5, pp. 949–964, May 2018.

[25] S. Hashemi, A. Kroker, L. Bobach, and D. Bartel, "Multibody dynamics of pivot slipper pad thrust bearing in axial piston machines incorporating thermal elastohydrodynamics and mixed lubrication model," *Tribology Int.*, vol. 96, pp. 57–76, Apr. 2016.

[26] A. Schenk and M. Ivantysynova, "A transient thermoelastohydrodynamic lubrication model for the slipper/swashplate in axial piston machines," *J. Tribol*, vol. 137, no. 3, Jul. 2015, Art. no. 031701.

[27] W. Shen, Y. Pang, and J. Jiang, "Robust controller design of the integrated direct drive volume control architecture for steering systems," *ISA Trans.*, vol. 78, pp. 116–129, Jul. 2018.

[28] K. Suzuki and E. Urata, "Development of a water hydraulic pressure-compensated flow control valve," *Int. J. Fluid Power*, vol. 9, no. 3, pp. 25–33, Jan. 2008.

[29] H. Yu, H. Li, Y. Li, and Y. Li, "A novel improved full vector spectrum algorithm and its application in multi-sensor data fusion for hydraulic pumps," *Measurement*, vol. 133, pp. 145–161, Feb. 2019.

[30] G. Haidak, D. Wang, and E. Shiju, "Research on the thermo-elastic deformation and fracture mechanism of the slipper retainer in the axial piston pumps and motors," *Eng. Failure Anal.*, vol. 100, pp. 259–272, Jun. 2019.

[31] R. C. Portillo, "Cylinder block/valve plate interface performance investigation through the introduction of micro-surface shaping," M.S. thesis, Dept. Mech. Eng., Purdue Univ., Lafayette, IN, USA, 2014, p. 119.

[32] I. V. Dobrov, "On the friction theory of solids with flat contact surface," *Procedia Eng.*, vol. 150, pp. 527–535, Jan. 2016.

[33] D. Wang, Y. Song, J. Tian, E. Shiju, and G. Haidak, "Research on the fluid film lubrication between the piston-cylinder interface," *AIP Adv.*, vol. 8, no. 10, Oct. 2018, Art. no. 105330.
[34] J. Zhang, Q. Chao, B. Xu, M. Pan, Q. Wang, and Y. Chen, "Novel three-piston pump design for a slipper test rig," *Appl. Math. Model.*, vol. 52, pp. 65–81, Dec. 2017.
[35] J. M. Bergada, J. Watton, J. M. Haynes, and D. L. Davies, "The hydrostatic/hydrodynamic behaviour of an axial piston pump slipper with multiple lands," *Meccanica*, vol. 45, no. 4, pp. 585–602, Aug. 2010.
[36] T. Kazama, M. Suzuki, and K. Suzuki, "Relation between sliding-part temperature and clearance shape of a slipper in swashplate axial piston motors," *JFPS Int. J. Fluid Power Syst.*, vol. 8, no. 1, pp. 10–17, 2014.

GASTON HAIDAK was born in Chugule, Cameroon, in 1993. He received the degree in general physics from the University of Yaounde 1, Cameroon, in 2015, and the degree in mechanical and electrical engineering from the Institute of Mine and Petroleum Industries (IMIP), University of Maroua, Cameroon, in 2017, where he became familiar with designs and simulations. He is currently pursuing the M.S. degree in computer intelligent control and electromechanical engineering with the College of Engineering, Zhejiang Normal University, China, with a focus on modeling and simulation to improve the efficiency of hydraulic machines.

DONGYUN WANG was born in 1981. He received the Ph.D. degree in mechanical engineering from the College of Mechanical Engineering, Zhejiang University, Hangzhou, China, in 2009, with a focus on hybrid power-train technology on construction machinery.

He was a Visiting Scholar with the Maha Fluid Power Research Center, Purdue University, USA, from 2014 to 2015. He is currently a Professor with the College of Engineering, Zhejiang Normal University, China. He has conducted several projects from the National Nature Science Foundation and Natural Science Foundation of Zhejiang Province. His current research interests include new type hydraulic components and smart manufacturing advanced design technology.

SHIJU E, photograph and biography not available at the time of publication.

FEIYUE LI, photograph and biography not available at the time of publication.